Calibration of Parallel Kinematic Devices Using Sequential Determination of Kinematic Parameters

Bernhard Jokiel, Jr., Sandia National Laboratories
Lothar Bieg, Sandia National Laboratories
John C. Ziegert, University of Florida Machine Tool Research Center

Sandia is a multiprogram laboratory operated by Sandia Corporation, a Lockheed Martin Company, for the United States Department of Energy under Contract DE-AC04-94AL85000.

---

1. Introduction

In PKM machines, the Cartesian position and orientation of the tool point carried on the platform is obtained from a kinematic model of the particular machine. Accurate positioning of these machines relies on the accurate knowledge of the parameters of the kinematic model unique to the particular machine. The parameters in the kinematic model include the spatial locations of the joint centers on the machine base and moving platform, the initial strut lengths, and the strut displacements. The strut displacements are readily obtained from sensors on the machine. However, the remaining kinematic parameters (joint center locations, and initial strut lengths) are difficult to determine when these machines are in their fully assembled state. The size and complexity of these machine generally makes it difficult and somewhat undesirable to determine the remaining kinematic parameters by direct inspection such as in a coordinate measuring machine. In order for PKMs to be useful for precision positioning applications, techniques must be developed to quickly calibrate the machine by determining the kinematic parameters without disassembly of the machine. A number of authors have reported techniques for calibration of PKMs (Soons[1,2], Masory, [3], Zhuang et.al.[4,5], Ropponen [6]) In two other papers [7, 11], the authors have reported on work recently completed by the University of Florida and Sandia National Laboratories on calibration of PKMs, which describes a new technique to sequentially determine the kinematic parameters of an assembled parallel kinematic device. The technique described is intended to be used with a spatial coordinate measuring device such as a portable articulated CMM measuring arm (Romer, Faro, etc.), a Laser Ball Bar (LBB), or a laser tracker (SMX, API, etc). The material to be presented is as follows: (1) methods to identify the kinematic parameters of 6-6 variant Stewart platform manipulators including joint center locations relative to the worktable and spindle nose, and initial strut lengths, (2) an example of the application of the method, and (3) results from the application of the technique.

2. Coordinate Reference Frames In Calibration

Many different coordinate reference frames are used during calibration. Some of these frames are exclusive to the machine being calibrated, other to the measurement device, and others for the calibration method itself (Figure 1). Table 1 contains a synopsis of each frame and location.

(Figure 1 here)

DISCLAIMER

DISCLAIMER

Portions of this document may be illegible in electronic image products. Images are produced from the best available original document.

Table 1 – Coordinate reference frame descriptions.

Name	Symbol	Purpose	Location
Tool	Tl	Machine controlled relative to M during motion programs	Origin coincident with tool tip Z axis coincident with spindle center line.
Spindle Nose	Sn	Machine spindle nose location.	Parallel to Tl, translated along spindle centerline to spindle flange.
Platform Joint	P	Machine platform joints.	For the machine configuration explored, the platform joints were nominally arranged in a circle. Therefore P was located at the center of the circle and plane formed by the platform joints and fixed relative to the platform. The location of this frame is dependent upon the particular machine architecture encountered.
Base Joint	B	Machine base joints.	For the machine configuration explored, the base joints were nominally arranged in a circle. Therefore B was located at the center of the circle and plane formed by the platform joints and fixed relative to the platform. The location of this frame is dependent upon the particular machine architecture encountered.
Machine Worktable	M	Fixed frame in which tool motion is controlled.	Fixed relative to machine, coincident with worktable surface. Origin and the X and Y axis directions arbitrarily located.
Measuring Device	Md	Frame inherent to measuring device.	Arbitrarily located relative to machine, but fixed during measurement cycle.
Central Reference	R	Fixed relative to M to which all spatial coordinates are transformed.	Formed by three targets affixed to the worktable.
Platform Reference	PR	Tracked by measuring device to determine motion of platform.	Arbitrarily located relative to M, but fixed relative to P, Sn andTl.

3. Establishing the Central Reference Frame (R)

In general, the measurement device may need to be moved to several different locations during the calibration process. However, all coordinate data collected by the device must be referenced to a common coordinate system. Therefore, it is necessary to have a temporary fixed reference frame (the central reference frame R) to which all of the spatial data collected in the various Md frames will be transformed. The R frame is constructed from three measurement target mounts (r_1, r_2, and r_3) secured at the farthest corners of the worktable Figure 2. The coordinates of each of the R targets are measured relative to one Md system several times.

(Figure 2 here)

Using the mean coordinate values for each target mount location measured in the Md system ($^{Md}r_1$, $^{Md}r_2$, and $^{Md}r_3$), the homogeneous coordinate transformation (HTM) $^{Md}T_R$ is constructed.

(1)

4. Locating the Machine (M) Coordinate Frame

Since the temporary R frame is arbitrarily located relative to the M frame, there is no guarantee that it is located in a sensible manner. In addition, it is desirable for the mechanism to move accurately in coordinates that are expressed relative to the worktable where part fixtures, raw stock, and ultimately the finished part are located. For these reasons it is necessary to determine the HTM between the R and the M frames to transform all measurements expressed in the temporary R frame into the permanent M frame.

Since PKM devices have no guideways to physically embody Cartesian motions (as in traditional orthogonal stacked guideway machines) there is a great deal of flexibility in defining the location of the M system. For this work, the M system is chosen to be located at the center of the worktable, coincident with the worktable plane, where the X-axis is parallel to the T-slots (+X to the right), and the Z-axis is parallel to the worktable surface normal (+Z pointing up). See Figure 2.

4.1. Defining the M Frame Z-axis Unit Vector

The Z-axis of the M system ($^{Md}z_M$) is parallel to the surface normal of the worktable. The worktable surface normal relative to the Md may be experimentally determined by finding the best-fit plane of several (as few as three) points on the flat surface of the table, avoiding the T-slots and obvious surface blemishes (Figure 3).

(Figure 3 here)

The residual function $\underline{f}(\underline{X})$ for the distance between a plane and a set of experimentally determined Cartesian points is:

$$\underline{f}(\underline{X}) = \begin{bmatrix} x_1 & y_1 & z_1 \\ \vdots & \vdots & \vdots \\ x_i & y_i & z_i \\ \vdots & \vdots & \vdots \\ x_m & y_m & z_m \end{bmatrix} \cdot \begin{Bmatrix} -n_x \\ -n_y \\ -n_z \\ D \end{Bmatrix} = A \cdot \underline{X} \qquad (2)$$

Applying the least squares method to $\underline{f}(\underline{X})$, the equation for the solution becomes:

$$A^T A \underline{X} = \underline{0} \qquad (3)$$

Thinking of this equation as an eigenvalue problem ($A^TA\underline{X}=\lambda\underline{X}$), it stands to reason that the eigenvector $\underline{X}_{\lambda=0}$ that corresponds to the eigenvalue $\lambda=0$ of the A^TA matrix would be the solution. The unit normal ($\underline{n}$) and the offset distance (D) from the origin to the plane may then be calculated.

$$ {}^{Md}\hat{z}_M = \underline{n} = \frac{-((\underline{X}_{\lambda=0})_1, (\underline{X}_{\lambda=0})_2, (\underline{X}_{\lambda=0})_3)}{\sqrt{(\underline{X}_{\lambda=0})_1^{\,2} + (\underline{X}_{\lambda=0})_2^{\,2} + (\underline{X}_{\lambda=0})_3^{\,2}}} $$

$$ D = \frac{(\underline{X}_{\lambda=0})_4}{\sqrt{(\underline{X}_{\lambda=0})_1^{\,2} + (\underline{X}_{\lambda=0})_2^{\,2} + (\underline{X}_{\lambda=0})_3^{\,2}}} \qquad (4) $$

4.2. Defining the M Frame X-axis Unit Vector

The X-axis of the M system ($^{Md}x_M$) is chosen to be parallel to the worktable T-slots. The direction of the T-slots may be experimentally determined by finding the best-fit 3D line from several (as few as two) points measured along one T-slot (Figure 4).

(Figure 4 here)

The direction vector ($\underline{S}$) and the moment ($\underline{S}_0$) about the origin of a line are:

$$ {}^{Md}\hat{x}_M = \underline{S} = \frac{(m_x, m_y, m_z)}{\sqrt{m_x^{\,2} + m_y^{\,2} + m_z^{\,2}}} $$

$$ \underline{S}_0 = (b_x, b_y, b_z) \times \underline{S} \qquad (5) $$

Applying the least squares method to the parametric equations of a 3D line:

$$ X(t) = m_x t + b_x \quad Y(t) = m_y t + b_y \quad Z(t) = m_z t + b_z \qquad (6) $$

m_x, m_y, m_z, b_x, b_y, and b_z, may be computed:

$$ \begin{bmatrix} m_x \\ b_x \end{bmatrix} = \left(\begin{bmatrix} 1 & \dots & i & \dots & n \\ 1 & \dots & 1 & \dots & 1 \end{bmatrix} \begin{bmatrix} 1 & 1 \\ \vdots & \vdots \\ i & 1 \\ \vdots & \vdots \\ n & 1 \end{bmatrix} \right)^{-1} \begin{bmatrix} 1 & \dots & i & \dots & n \\ 1 & \dots & 1 & \dots & 1 \end{bmatrix} \begin{bmatrix} x_1 \\ \vdots \\ x_i \\ \vdots \\ x_n \end{bmatrix} \qquad (7) $$

(two other similar relations involving m_y, m_z, b_y, and b_z are not shown)

4.3. Defining the M Frame Y-axis Unit Vector

The Y-axis unit vector ($^{Md}y_M$) is the cross product of the M frame Z and X-axis unit vectors.

$$ {}^{Md}\hat{y}_M = {}^{Md}\hat{z}_M \times {}^{Md}\hat{x}_M \qquad (8) $$

4.4. Defining the M Frame Origin

Once the desired location of the origin of the M frame is selected, the location of this point is measured relative to the Md system. The measured point however may not lie exactly in the plane of the table. To assure that the coordinates of the origin are in the plane of the worktable the coordinates of the measured point are projected into the worktable's best-fit plane. The coordinates of the projected point in the plane constitute the location of the origin of the machine frame ${}^{Md}O_M$ (Figure 5).

(Figure 5 here)

$$ {}^{Md}O_M = {}^{Md}O + \left(D - {}^{Md}\hat{z}_M \cdot {}^{Md}O\right){}^{Md}\hat{z}_M \tag{9} $$

4.5. Expressing the M Frame Relative to the R Frame

All of the information necessary to determine the HTM (${}^{Md}T_M$) has been experimentally determined, and may be assembled:

$$ {}^{M}T_{Md} = \begin{bmatrix} {}^{Md}\hat{x}_M & {}^{Md}\hat{y}_M & {}^{Md}\hat{z}_M & {}^{Md}\underline{O}_M \\ 0 & 0 & 0 & 1 \end{bmatrix} \tag{10} $$

The transformation relating the R system to the M frame (${}^{M}T_R$) may be calculated from the previously determined transformations ${}^{Md}T_M$ and ${}^{Md}T_R$.

$$ {}^{M}T_R = {}^{M}T_{Md} \cdot {}^{Md}T_R \tag{11} $$

5. Locating the Joint Centers of Rotation

The platform is moved along an arbitrary predetermined path while holding each strut in turn at an arbitrary fixed length. As the platform moves, the fixed-length strut rotates in its joints. During this motion, an arbitrary point on the strut will trace a path on a spherical shell relative to the strut's joint center of rotation, assuming that the joint produces spherical motion and there is negligible strut bending. Knowing this, the spatial coordinates of a measurement target affixed to a strut during this spherical movement are measured. By fitting the collected spatial coordinates of the target affixed to the strut to the equation of a sphere, the location of the center of the sphere and hence the location of the joint's center of rotation may be determined. This can readily be envisioned for the base joint (Figure 6). However by collecting the platform orientation and location information in addition to the strut gage point locations, the spatial gage point locations may be transformed into a coordinate system fixed relative to the platform system, allowing the location of the strut's platform joint center to be identified (Figure 7). By performing this procedure once for each of the six struts, the locations of the base and platform joint centers of rotation may be identified for all of the six struts. The flow chart for the joint center identification process is shown in (Figure 8)

(Figure 6 here)

(Figure 7 here)

(Figure 8 here)

5.1. The Strut Target Fixture

The strut fixture holds two measurement target mounts (S_A and S_B). The centers of S_A and S_B are arranged so that they are equidistant from the strut centerline and a line joining these points passes through the strut centerline (Figure 9).

(Figure 9 here)

In this configuration, the coordinates of S_A and S_B may be averaged to calculate the coordinates of a virtual point (S_M) on the neutral axis of the strut. This is desirable to remove the effects of strut bending due to friction in the joints from the collected data (Figures 10a and 10b). If a strut were to bend during data collection, a target attached to the strut, but not on the neutral axis, would translate radially relative to the joint center, causing what would appear to be nonspherical joint motion.

(Figure 10 here)

5.2. The Platform Target Fixture and PR Frame

The method depends on repeatedly measuring a coordinate system (PR) attached to the platform (see Figure 8). Therefore it is essential that the fixtures holding the targets on the platform are stiff, secure and thermally stable, and are not moved relative to the platform during the entire measurement process. When designing the fixtures and setting up for the measurement cycle, it is important to keep in mind that all of the targets (r_1, r_2, r_3, S_A, S_B, pr_1, pr_2, and pr_3) must be visible to the chosen measuring instrument at all times for all motion paths.

5.3. Path Motion Planning

The objective is to create a motion program that will move the spindle nose in space while holding a particular strut at an arbitrary fixed length. The path which the i^{th} platform joint ${}^{M}P_i$ is to follow must satisfy the mobility constraints of the particular machine (strut extension and joint limits, obstructions in the workvolume such as tool changers, etc.) and the workspace of the particular measuring instrument used. However the path points are chosen (simulation, or trial and error), every point ${}^{M}P_{i,j}$ on the path must satisfy the equation of the sphere to guarantee that the strut length remains constant at each point on the path.

Once the platform joint path is chosen, the corresponding spindle nose position for each path point must be calculated. The first step in this process is to select the orientation of the platform about the (x,y,z) axes of the M system at each point on the path. The orientation may be constant for all points, or may be allowed to vary from point to point. In any case, the orientation ${}^{M}(\alpha,\beta,\gamma)_j$ for the j^{th} path point has the rotation matrix:

$$\left({}^{M}R_{P}\right)_{j}=\begin{bmatrix}\cos\beta\cos\gamma+\sin\alpha\sin\beta\sin\gamma & -\sin\beta\sin\gamma+\sin\alpha\sin\beta\cos\gamma & \cos\alpha\sin\beta\\ \cos\alpha\sin\gamma & \cos\alpha\cos\gamma & -\sin\alpha\\ -\sin\beta\cos\gamma+\sin\alpha\cos\beta\sin\gamma & \sin\beta\sin\gamma+\sin\alpha\cos\beta\cos\gamma & \cos\alpha\cos\beta\end{bmatrix} \quad \textbf{(12)}$$

Knowing the nominal position of the spindle nose position relative to the chosen platform joint center, the location of the spindle nose that will hold the strut at the nominal desired length is:

$$\left({}^{M}Tl\right)_{i,j}=\left({}^{M}P\right)_{i,j}+\left({}^{M}R_{P}\right)_{j}\left(\left({}^{P}Tl\right)_{i,j}-\left({}^{P}P\right)_{i}\right) \quad \textbf{(13)}$$

It is important to note here that the path developed using this method does not require accurate values for the kinematic parameters of the machine being calibrated. However, it is critical that the

kinematic parameters used in the machine's controller identically match the ones used to create the motion path. If the kinematic parameters in the controller do not identically match the ones used to create the spindle nose path, constant strut length cannot be maintained.

5.4. Least Squares Fit to Equation of a Sphere

In the case of fitting a set of "n" experimentally determined Cartesian coordinate triples to the equation of a sphere, the equation for the residual "$\underline{f}(\underline{X})$" is:

$$\underline{f}(\underline{X}) = \begin{bmatrix} x_1 & y_1 & z_1 & 1 \\ \vdots & \vdots & \vdots & \vdots \\ x_i & y_i & z_i & 1 \\ \vdots & \vdots & \vdots & \vdots \\ x_n & y_n & z_n & 1 \end{bmatrix} \cdot \begin{Bmatrix} 2h \\ 2k \\ 2l \\ C \end{Bmatrix} - \begin{Bmatrix} x_1^2 + y_1^2 + z_1^2 \\ \vdots \\ x_i^2 + y_i^2 + z_i^2 \\ \vdots \\ x_n^2 + y_n^2 + z_n^2 \end{Bmatrix} = A \cdot \underline{X} - \underline{b} \qquad (12)$$

$$where: \quad C = r^2 - h^2 - k^2 - l^2$$

The minimum value of the sum of squares of the residual is $\underline{X}$, where:

$$\underline{X} = (A^T A)^{-1} A^T \underline{b} \qquad (13)$$

The coordinates of the center (h,k,l) and radius (r) are:

$$h = -\frac{X_1}{2} \quad k = -\frac{X_2}{2} \quad l = -\frac{X_3}{2} \quad r = \sqrt{X_4 + h^2 + k^2 + l^2} \qquad (14)$$

5.5. Detecting Probable "Bad" Data Points

A method of rejecting bad data points was needed to identify and remove measurements from the data sets that were inaccurately measured. This was accomplished by checking the invariant inter-target distance between the strut gage points (S_A,S_B), and the invariant inter-target distances between the platform gage points (pr_1, pr_2, pr_3). For each pose, the distances SA-SB, pr_1-pr_2, pr_1-pr_3, and pr_2-pr_3 were calculated. Their respective means were calculated over all of the poses for the corresponding strut data set. The deviation from the mean for each inter-target distance for every pose in the set was calculated. Poses where one or more of the distance deviations were greater than a chosen threshold value were eliminated from the data set. The set of acceptable data points was then fit to the equation of a sphere. Figure 11 shows a graph of the inter-target distances for strut 1 trial 1 before the rejection of bad data points. The horizontal lines are the limits set for the allowable deviation from the mean. For the S_A- S_B distances this limit is 0.018mm, and for the PR distances it is 0.013mm. Note the deviation in S_A- S_B that appears at poses 2, 19 and 20. Since the deviations from the mean are larger than the limits, these poses will be removed before the data is fit to a sphere.

(Figure 11 here)

6. Locating the Spindle Nose

The location of the spindle nose and the orientation of the centerline relative to the joint centers must be determined. This is achieved by tracking the rotation of the spindle relative to the PR system. Assuming that the spindle exhibits negligible axial and radial motion, the circular plane defines the spindle's orientation and nose center position (Figure 12).

(Figure 12 here)

6.1. Tracking Spindle Rotation

A stiff fixture holding a measurement target (S_R) is attached to a tool holder. The axial offset distance of the tool holder target relative to the tool holder-spindle flange is determined by a CMM (see Figure 12), and the tool holder and fixture assembly is inserted into the spindle. The platform is held in a fixed pose from which the measuring device can reach the PR gage points and S_R. The coordinates of the PR gage points are each measured several times, averaged and the HTM ${}^{Md}T_{PR}$ is computed (see Section 2). The spindle is rotated slowly by hand. At approximately 30-40 uniformly distributed locations, the spindle rotation is stopped, and the coordinates of the gage point S_R are measured relative to the Md system ${}^{Md}(S_R)$.

The coordinates ${}^{Md}(S_R)$ are transformed into ${}^{PR}(S_R)$:

$$ {}^{PR}S_R = \left({}^{Md}S_{PR}\right)^{-1} {}^{Md}S_R \tag{15} $$

The coordinates ${}^{PR}(S_R)$ are fit to a plane (see Section 3) and a circle in the best-fit plane. The fit to a circle is essentially the same as that of a sphere without the "z" component (see Section 4.4). The unit normal vector of the best-fit plane is the unit orientation vector of the spindle relative to the P system (${}^{PR}z_{Sn}$). The coordinates of the center of the circle projected along the positive direction of the normal vector by the offset distance are the coordinates of the center of the spindle (see Figure 13).

6.2. Expressing the Platform Joint Centers Relative to the Spindle

If it is desired to express the locations of the platform joints relative to the spindle nose, the appropriate HTM may be calculated from the following steps:

1. Compute the angle ϕ between the ${}^{PR}z_P$ and ${}^{PR}z_{Sn}$:

$$ \phi = \arccos({}^{PR}\hat{z}_P \cdot {}^{PR}\hat{z}_{Sn}) \tag{16} $$

2. If $\phi > 0$, compute the normal vector $\underline{n}$ from the cross product of ${}^{PR}z_P$ and ${}^{PR}z_{Sn}$:

$$ \underline{n} = {}^{PR}\hat{z}_{Sn} \times {}^{PR}\hat{z}_P \tag{17} $$

3. Compute the rotation matrix ${}^{Sn}R_P$ from the rotation ϕ degrees about $\underline{n}$:

$$ {}^{Sn}R_P = \begin{bmatrix} n_x n_x v + c & n_x n_y v - n_z s & n_x n_z v + n_y s \\ n_x n_y v + n_z s & n_y n_y v + c & n_y n_z v - n_x s \\ n_x n_z v - n_y s & n_y n_z v + n_x s & n_z n_z v + c \end{bmatrix} \tag{18} $$

$$ c = \cos(\phi) \quad s = \sin(\phi) \quad v = 1 - \cos(\phi) $$

4. Compute the coordinate difference between the frame origins ${}^{PR}P_O$ and ${}^{PR}Sn_O$:

$$\Delta O = {}^{PR}P_O - {}^{PR}Sn_O \tag{19}$$

5. Assemble ${}^{Sn}T_P$:

$${}^{Sn}T_P = \begin{bmatrix} \left[{}^{Sn}R_P\right]_{3x3} & \Delta O_{3x1} \\ 0 \quad 0 \quad 0 & 1 \end{bmatrix} \tag{20}$$

6. Premultiply the platform coordinate location by the inverse of ${}^{Sn}T_P$:

$${}^{P}P = \left({}^{Sn}T_P\right)^{-1}{}^{Sn}P \tag{21}$$

7. Determining the Initial Strut Lengths

Calculating the initial strut reference lengths proceeds as follows. The machine's homing routine is executed. With the platform retracted to its home position, the coordinates of the PR gage points are measured relative to the Md system. The coordinate transformations $({}^{Md}T_{PR})_1$ and $({}^{M}T_{PR})_1$ are calculated. The platform joint center coordinates and the base joint center coordinates are all expressed in the M frame using these transformations, and the distances between the each of the six strut joint pairs $(L_{init})_{j=1 \text{ to } 6}$, are calculated from the formula for straight line distance. The platform is then moved from its home location, and the process is repeated several times. The initial strut reference length for each strut is taken to be the mean of the calculated strut lengths for each strut over all of the trials (Figure 13).

(Figure 13 here)

8. Experimental Results

The candidate machine for the calibration was a Hexel Tornado 2000 milling machine. The Tornado 2000 is a 6-3 Stewart platform design, with a $1m^3$ workvolume. The struts are rollerscrews (20mm diameter with a 5mm pitch). The encoders have 10,000 counts providing a least count of 0.0005mm on each strut.

The spatial measurement device used was a SMX 4000 laser tracker. Utilizing a heterodyne laser interferometer and two rotary encoders, the accuracy of the tracker within the 2-3m workvolume is less than 0.020mm of true position.

Three independent trials of the sequential determination method were performed and three new databases for the machine tool controller were constructed. The values for the kinematic parameters obtained from the calibration trials are shown in *(Table 2)* along with the values used by the machine manufacturer.

Table 2 – Results for kinematic parameters

Trial	Strut	Number of Data Points Used	Base Joint Locations X (mm)	Y (mm)	Z (mm)	Platform Joint Locations X (mm)	Y (mm)	Z (mm)	Initial Strut Length (mm)
1	1	17	123.432	351.049	1292.519	149.860	86.865	306.988	456.708
	2	18	408.542	-144.972	1292.796	149.818	86.896	306.892	455.324
	3	13	285.984	-355.838	1293.249	0.816	-173.854	308.318	455.428
	4	16	-286.048	-354.743	1294.499	0.909	-173.846	308.243	454.211
	5	19	-407.419	-143.216	1294.304	-150.216	86.892	305.697	457.072
	6	19	-120.656	351.557	1293.139	-150.259	86.842	305.865	459.985
2	1	14	123.462	351.057	1292.543	149.903	86.900	306.885	456.657
	2	17	408.558	-144.981	1292.754	149.869	86.881	306.835	455.198
	3	18	286.069	-355.859	1293.235	0.936	-173.884	308.242	455.37
	4	20	-286.054	-354.746	1294.468	0.930	-173.864	308.240	454.096
	5	19	-407.450	-143.224	1294.330	-150.229	86.876	305.569	457.135
	6	16	-120.726	351.510	1293.134	-150.262	86.786	305.672	460.006
3	1	17	123.486	351.078	1292.451	149.881	86.893	306.882	456.567
	2	18	408.560	-144.954	1292.742	149.817	86.886	306.752	455.282
	3	20	286.074	-355.860	1293.333	0.838	-173.850	308.223	455.47
	4	16	-286.075	-354.807	1294.455	0.875	-173.811	308.115	454.239
	5	19	-407.450	-143.199	1294.252	-150.357	86.883	305.738	456.969
	6	18	-120.703	351.536	1293.123	-150.273	86.907	305.724	459.928
Orig.	1	-	121.847	353.309	1291.396	150.219	86.760	306.547	456.654
	2	-	408.005	-142.071	1291.500	150.219	86.760	306.547	460.297
	3	-	285.667	-353.347	1291.550	1.203	-173.892	308.188	455.489
	4	-	-286.289	-353.168	1291.483	1.203	-173.892	308.188	459.225
	5	-	-408.011	-142.071	1291.500	-149.827	86.760	305.785	457.287
	6	-	-122.262	353.384	1291.500	-149.827	86.760	305.785	460.009

Although it would be desirable to compare the experimentally determined values of the kinematic parameters to the true values, this is not possible since the true values are unknown. Therefore, the quality of the experimentally determined kinematic model parameters is evaluated by using a standard machine accuracy performance test. The test chosen is the circular trace test described in ANSI/ASME B5.54, Performance Evaluation of Computer Numerically Controlled Machining Centers [8]. These tests were performed using a telescoping magnetic ballbar manufactured by Renishaw (Figure 14).

(Figure 14 here)

The three new sets of kinematic parameters and the original set were verified using a series of six circular traces (Table 3) for a total of 24 recorded traces.

Table 3.6 – Locations and radii of circular traces.

Trace	Nominal Center Position (mm)	Radius (mm)
1	(0, 0, 180)	150
2	(200, 200, 180)	150
3	(-200, 200, 180)	150
4	(-200, -200, 180)	150
5	(200, -200, 180)	150
6	(0, 0, 180)	300

For each circle trace, a quality index (QI) was calculated.

$$QI(mm) = \frac{Radial\ Deviation_{Max} - Radial\ Deviation_{Min} + \sqrt{x_{center}^{\ 2} + y_{center}^{\ 2}}}{1000} \quad \textbf{(22)}$$

For each trial, the mean and range (maximum – minimum) of the QI was calculated (Table 4). Trial 1 exhibits the lowest QI mean and range of the four databases tested, which indicates that of the four databases, Trial 1 has the best overall performance based on the verification tests performed.

Table 4 – Quality index for each trial/circle combination.

Circle	Original Database (mm)	Trial 1 Database (mm)	Trial 2 Database (mm)	Trial 3 Database (mm)
1	0.101	0.084	0.097	0.087
2	0.106	0.081	0.132	0.072
3	0.158	0.096	0.110	0.069
4	0.093	0.114	0.074	0.143
5	0.154	0.108	0.094	0.121
6	0.145	0.103	0.140	0.138
Mean	0.126	**0.098**	0.108	0.105
Range	0.065	**0.033**	0.066	0.075

9. Summary and Conclusion

The method proposed has four steps: locating the worktable, locating the joint centers, locating the spindle relative to the platform joints, and determination of the initial strut lengths. Although this method was only tested on one type of a Stewart platform device (6-3), there are no machine specific limitations which would prevent the method from being adapted to other Stewart platform devices,

and may possibly be used to calibrate other kinematic parallel devices not based on Stewart platforms. A secondary goal of the method development was to not rely on precision artifacts such as ring gages or ballplates. Although some fixtures were fabricated to attach the laser tracker targets mounts to the machine, they were inexpensive and were not precision artifacts.

The method was successfully performed a total of three times on a Hexel Tornado 2000 milling machine using a SMX laser tracker. Each trial took two-eight hour days for one person to collect the required data. Methods to reject bad data points also had to be created to remove suspect data from the measurements. All of the kinematic parameters were successfully recovered in all three trials. Three new machine databases were created out of these three sets of kinematic parameters and were implemented in the Hexel's controller. Dynamic Renishaw ball bar circles were performed in six locations with two radii (150mm and 300mm) to determine the difference in machine performance between the three new parameter sets and the original parameter set.

Given the amount of preplanning and calculation required, the somewhat time consuming data collection, and the need for a high precision spatial coordinate measuring device required to collect the data, this method with some fine tuning still is a viable technique to calibrate fully assembled Stewart platform machines in the field. Although these may seem to be shortcomings of this method, they are merely difficulties which may be solved or avoided altogether with good computer programming and the next generation of spatial coordinate measuring devices, and do not appear to be major flaws which would make this method undesirable or impractical.

10. References

1. Soons, J.A., "Measuring the geometric errors of a hexapod machine tool", *Laser Metrology and Machine Performance IV, Proceedings of the 4th Lamdamap Conference,* Computational Mechanics Publications, 1999.

2. Soons, J.A., "Error analysis of a hexapod machine tool", *Laser Metrology and Machine Performance III, Proceedings of the the 3rd Lamdamap Conference,* Computational Mechanics Publications, 347-358, 1997.

3. Masory, O., et.al., "On the accuracy of a Stewart platform-Part II: Kinematic calibration and compensation." Proceedings of the IEEE International Conference on Robotics and Automation, pp. 725-731, 1993.

4. Zhuang, H., and Roth, Z.S., "Method for kinematic calibration of Stewart platforms", *Journal of Robotic Systems*, 10(3), 391-405, 1993.

5. Zhuang, H., and Liu, L., "Self-calibration of a class of parallel manipulators", *Proceedings of the IEEE International Conference on Robotics and Automation*, 994-999, 1996.

6. Ropponen, T., and Arai, T., "Accuracy analysis of a modified Stewart platform manipulator", *Proceedings of the IEEE International Conference on Robotics and Automation,* 521-525, 1995.

7. Jokiel, B., and Ziegert, J.C., "Sequential Determination of Kinematic Parameters in Assembled Stewart Platform Manipulators", *Proceedings of 1999 ASPE Annual Meeting*, Monterey, CA, November, 1999, pp. 457-461.

8. Zhuang, H., Li, B., and Roth, Z., "Self-calibration and mirror center offset elimination of a multi-beam laser tracking system", *Journal of Robotic and Autonomous Systems*, 9, 255-269, 1992.

9. Zhuang, H. and Roth, Z., "Modeling gimbal axis misalignments and mirror center offset in a single beam laser tracking measurement system", *Int. Journal of Robotics Research*, 14(3), 211-224, 1995.

10. Jokiel, B., Ziegert, J.C., Bieg, L.F.X., "Uncertainty Propagation in Calibration of Parallel Kinematic Machines," Submitted to *Precision Engineering* for review January 2000

FIGURES

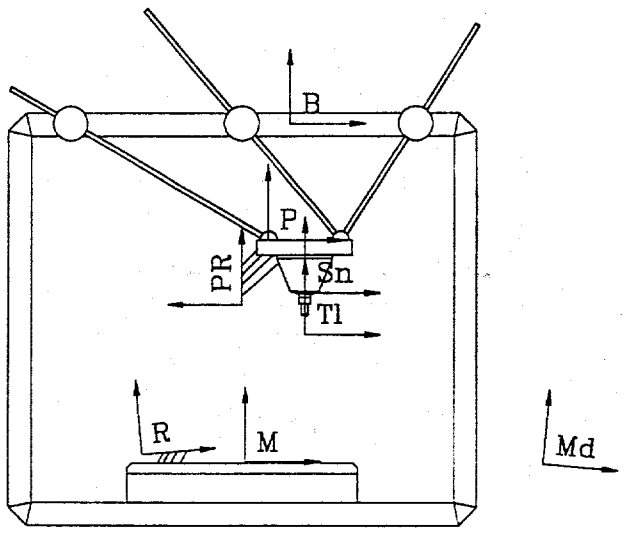

Figure 1 – Location of the various coordiante reference frames required.

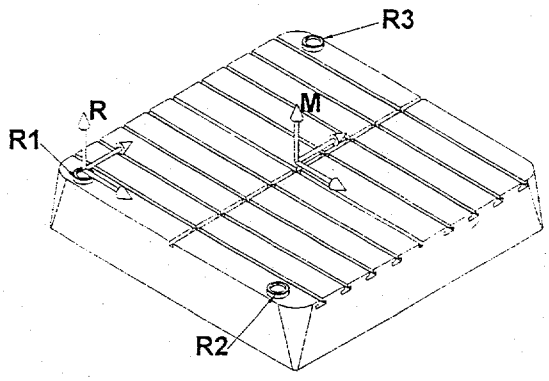

Figure 2 – Location of R and M reference frames.

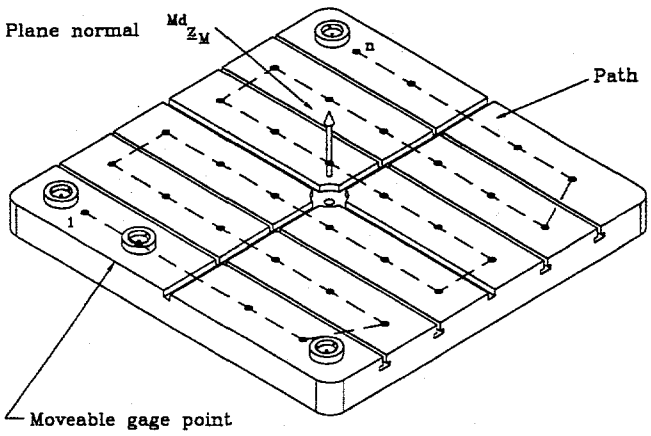

Figure 3 – Defining the M-system, Z-axis unit vector.

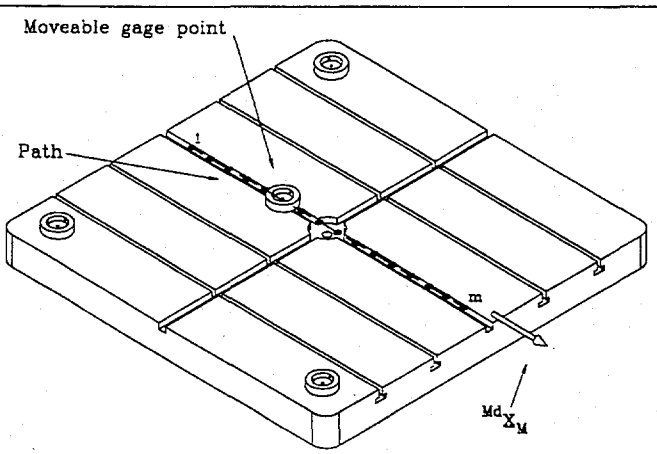

Figure 4 – Defining the M-system, X-axis unit vector

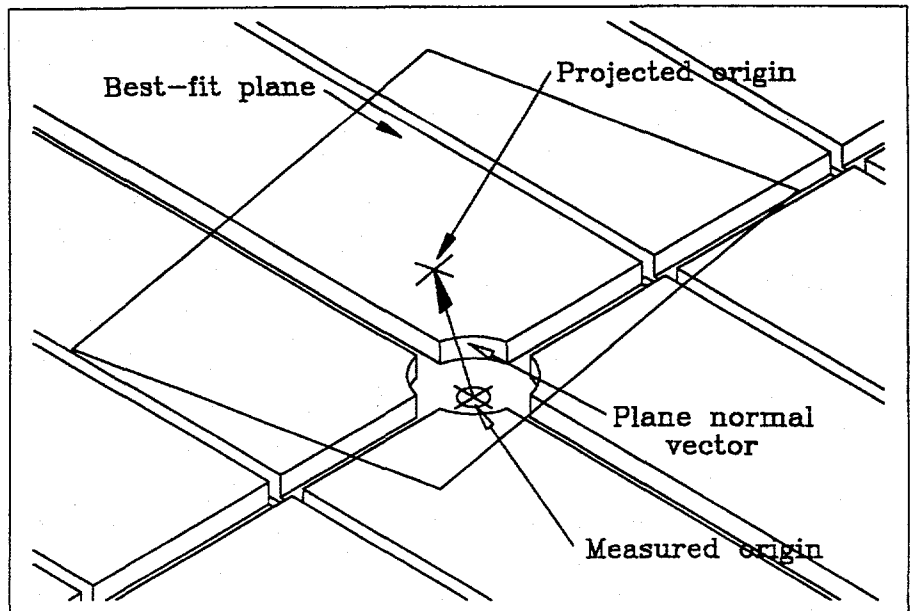

Figure 5 – Defining the M-system origin.

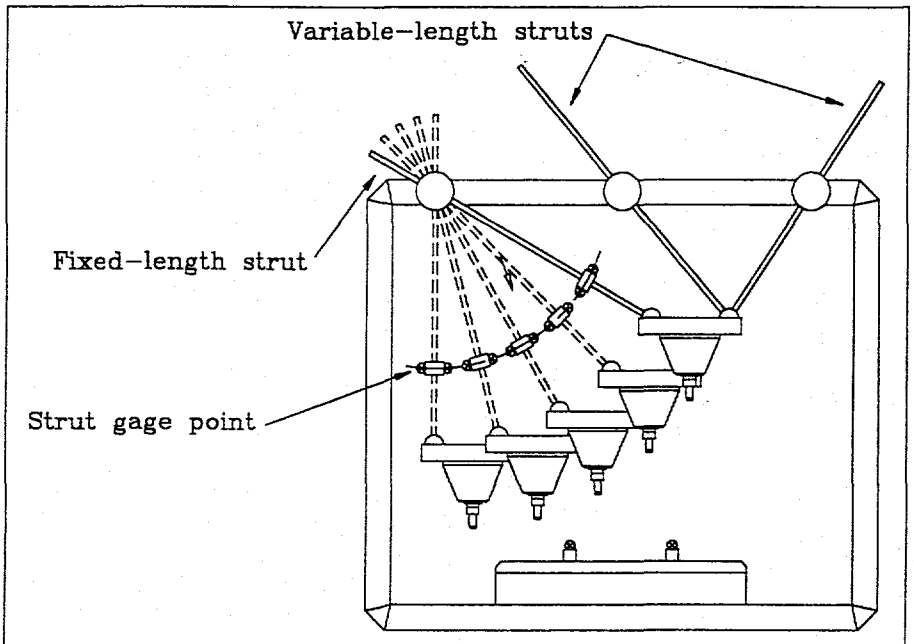

Figure 6 – Platform motion as seen relative to the M-system.

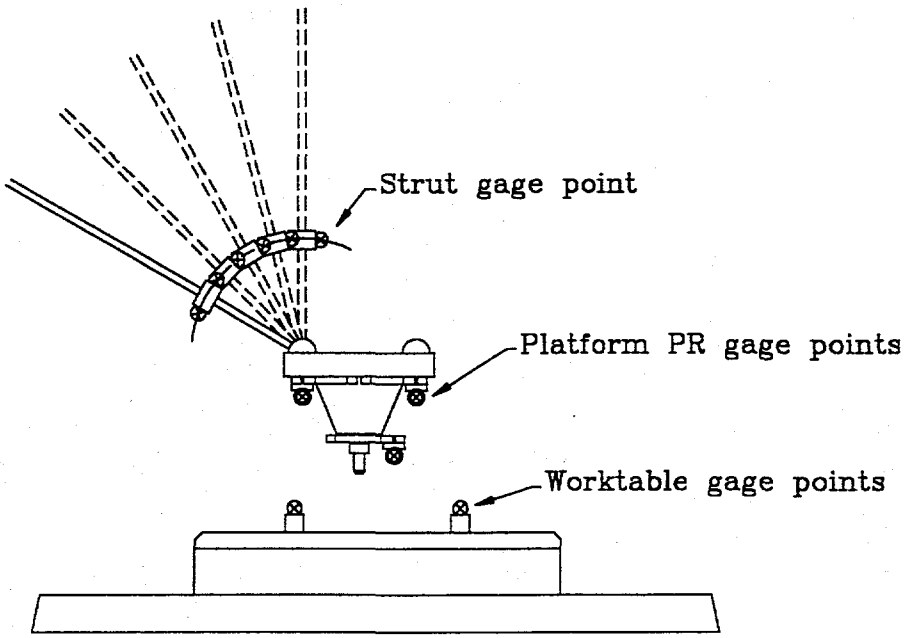

Figure 7 – Platform motion as seen relative to the P-system.

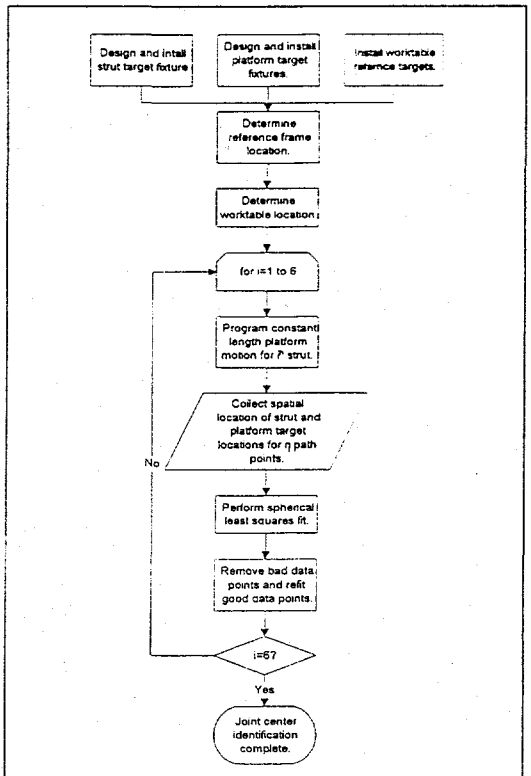

Figure 8 – Flowchart for joint location determination process.

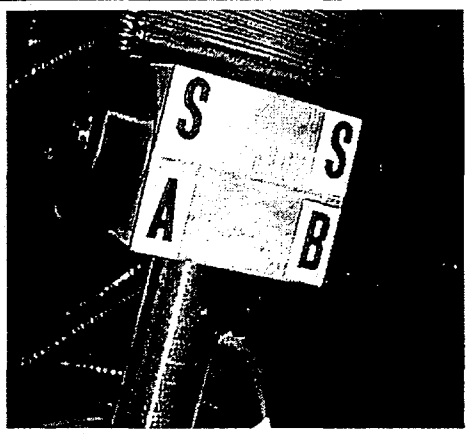

Figure 9 – Photograph of strut fixture where the vector joining S_A and S_B intersects the strut centerline vector.

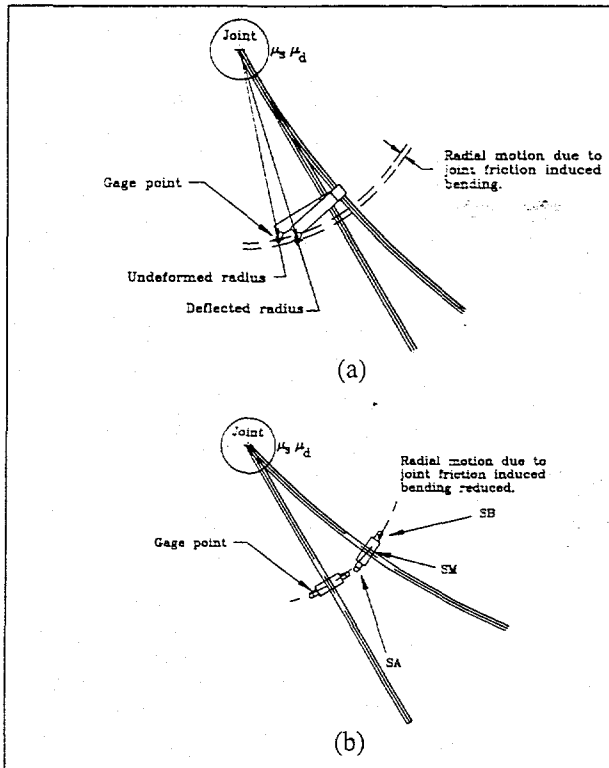

Figure 10 – (a) Effect of strut bending on cantilevered target. (b) Effect of strut bending on strut centerline-symmetric targets.

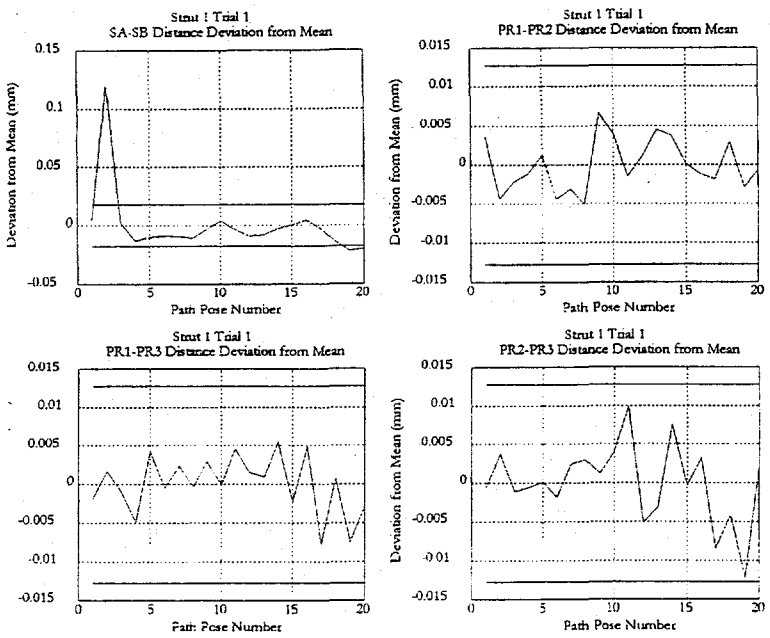

Figure 11 – Computed intertarget distances from experimental data.

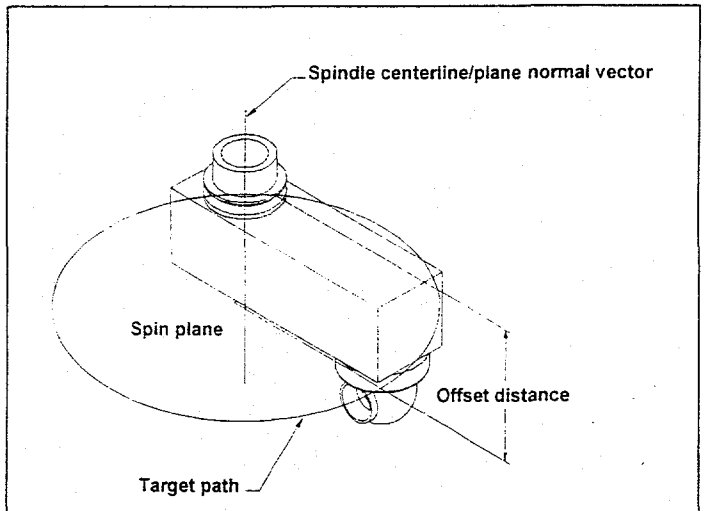

Figure 12 – Spindle fixture and target motion path to determine the spindle nose and centerline

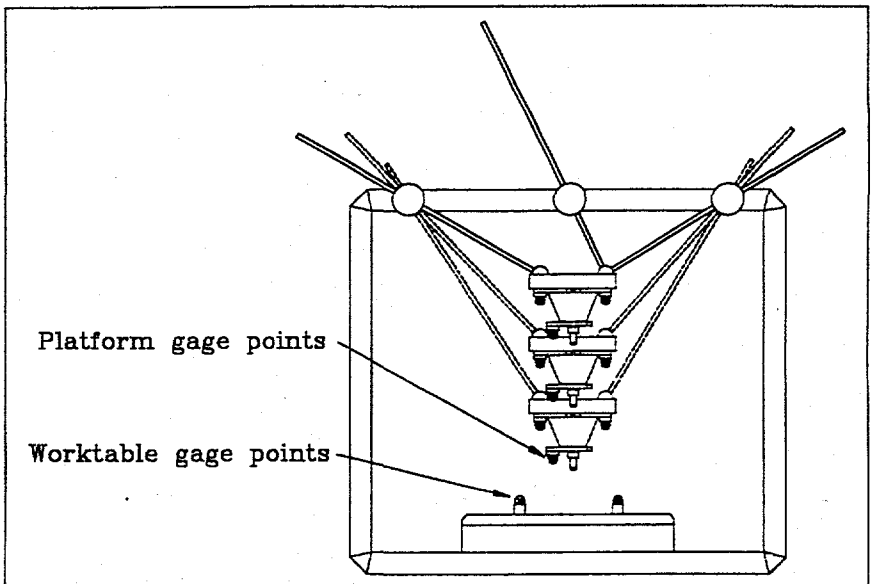

Figure 13 – Platform motion during homing sequence to determine initial strut lengths.

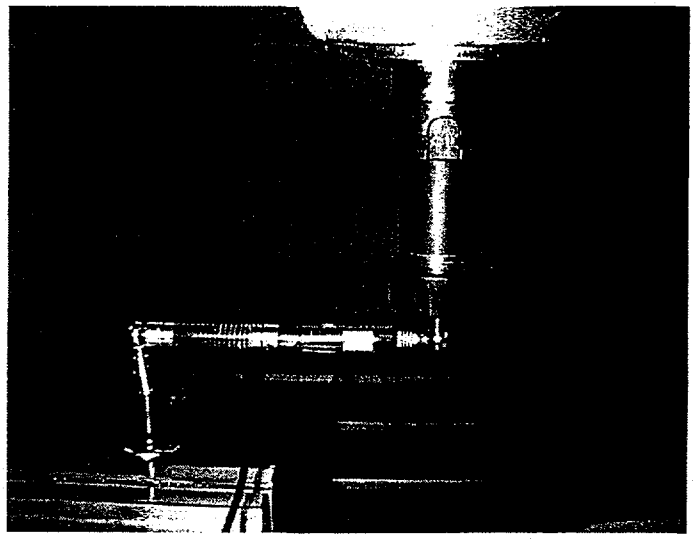

Figure 14 – A Renishaw magnetic ball bar was used to verify the circular tool paths.